Submitted to Physical Review B

LBL-1124
Preprint

A SYSTEMATIC EVALUATION OF THE SENSITIVITY OF LEED CALCULATIONS TO SMALL VARIATIONS OF THE INPUT PARAMETERS FOR THE ALUMINUM (100) SURFACE

M. R. Martin and G. A. Somorjai

August 1972

AEC Contract No. W-7405-eng-48

LBL-1124

DISCLAIMER

A SYSTEMATIC EVALUATION OF THE SENSITIVITY OF LEED CALCULATIONS TO SMALL VARIATIONS OF THE INPUT PARAMETERS FOR THE ALUMINUM (100) SURFACE

M. R. Martin and G. A. Somorjai

Department of Chemistry of the University of California at Berkeley
and Inorganic Materials Research Division
Lawrence Berkeley Laboratory, Berkeley, California 94720

ABSTRACT

Intensity-vs-incident electron energy (I-vs-eV) curves are obtained for the (00)-, (11)-, and (20)-beams diffracted from the (100) surface of aluminum. The beam intensities, calculated using a t-matrix formalism, are sensitive to small variations in the input parameters [number of phase shifts and atomic layers, order of multiple scattering, Debye temperature, incident beam angle, inner potential models and position of the surface atoms]. The use of low energy electron diffraction for surface structure determination depends on the sensitivity of the I-vs-eV curves to small variations of the surface geometry. The reliability of this method depends on the lack of sensitivity of these calculated curves to variations of the non-geometrical input parameters consistent with our knowledge of the physical processes involved. We conclude that the two most sensitive input parameters are variations in the incident beam angle and small displacements of the surface layer perpendicular to the surface. The inclusion of three layers parallel to the surface and five phase shifts are sufficient to obtain reliable calculated I-vs-eV curves for the (100) face of aluminum. The use of a Debye temperature for the surface layer which is smaller than that of the bulk layers is shown to attenuate the I-vs-eV curves uniformly. Exclusive reliance on a peak position or on relative peak intensities appears to be unjustified due to unresolved uncertainties in the models for the ion-core potential and for the electron self-energy correction. Displacement of the surface layer parallel to the surface is shown to have the greatest effect on the shape of the non (00)-beams intensity curves appearing in the direction of the displacement.

Introduction

Encouraging progress has been made recently on the problem of crystal surface structure analysis by low energy electron diffraction (LEED). Several theoretical approaches to the multiple scattering problem have led to the assembly of a variety of computer programs whose results have appeared recently in the literature. Multiple scattering has been taken into account by calculations based on a band structure approach[1-3], a t-matrix approach[4-6], and the layer KKR method[7,8]. In addition, two perturbation methods have been proposed to reduce the computer time requirements of the more exact methods[9-11]. It is the purpose of this paper to present the results of a detailed series of calculations on several beams diffracted from one face of a metal single crystal. We examine the behavior of the diffracted beam intensity peak positions and relative amplitudes as a function of the incident electron energy while varying the values of the input parameters furnished to the computation. In this way we seek to determine the sensitivity of LEED calculations to small variations in the physical and geometrical parameters supplied, and to determine the reliability of surface structure assignments obtained by this method. In this paper we report on LEED calculations made for the (100) surface of aluminum because of the relatively simple nature of this metal for which a number of calculations have already been made employing a variety of different approximations[7,9,10,12]. Calculations for the (110) and (111) surfaces are now in progress and will be reported later.

In section I, we describe the computer program we have developed and its limitations. Section II contains a comparison of results obtained by

the inclusion of different numbers of energy dependent phase shifts used to characterize the ion-core potential of the metal. In section III we investigate the effect of performing the calculation including different numbers of layers parallel to the surface. In section IV we show results of carrying out the calculation to various orders of multiple diffraction and investigate the effects of including a layer dependent Debye temperature. The sensitivity of the computed intensity curves to small variations in the incident beam angle near normal incidence is discussed in section V. Section VI presents a discussion of several methods for representing the energy dependence of the inner potential and compares the results obtained from them. Finally, in section VII we perform a number of variations of the lattice geometry in order to test the sensitivity of the calculated intensity curves to small displacements of the outermost layer, and comparisons are made with experimental results. All calculations reported in this paper are carried out for a lattice at room temperature, T = 293 K.

Results of these calculations show that a surface layer placed at an interlayer spacing equal to the bulk value $\pm$ 0.1 Å yields LEED intensity curves in good agreement with experimental curves for the (00), (11), and (20) beams of the aluminum (100) surface. Uncertainties in the values of the various input parameters presently limit our ability to state that the surface layer spacing actually lies within these limits. At the present state of LEED calculations it is meaningful to compare qualitatively the theoretical and experimental curves using both peak position and intensity information. Excessive reliance on either the peak positions or

the relative peak intensities exclusively appears to be unjustified in the light of unresolved questions regarding the values of certain input parameters that must be supplied to the calculation. Surface layer displacements of 0.2 Å parallel to the surface are shown to produce significant changes only in non-(00) beams whose observed spot pattern is parallel to the displacement. This directional dependence of the non-(00) beams should prove to be an aid in establishing the horizontal placement of surface atoms in overlayer systems and reconstructed surfaces.

I. Description of calculation

The computer program we have developed is based on the t-matrix approach to the multiple scattering problem as formulated by Beeby[4], and extended by Duke and Tucker[5] to include inelastic damping of the electron beam. The outgoing beams each correspond to a two dimensional reciprocal lattice vector $\underset{\sim}{g}$ in the plane of the surface, and we consider only the elastic case where E represents the incident and emerging electron energy. The number of electrons scattered elastically into the beam labelled by $\underset{\sim}{g}$ is proportional to the scattering cross section, $\sigma(\underset{\sim}{g},E)$,

$$\sigma(\underset{\sim}{g},E) = \frac{m^2}{(2\pi h^2)^2} \left| I_{\underset{\sim}{g}}(\underset{\sim}{k}_f,\underset{\sim}{k}_i;E)\right|^2, \qquad (1)$$

where

$$I_{\underset{\sim}{g}}(\underset{\sim}{k}_f,\underset{\sim}{k}_i;E) = \frac{(2\pi)^2}{A}\,\delta(\underset{\sim}{k}_{f_{\shortparallel}} - \underset{\sim}{k}_{i_{\shortparallel}} - \underset{\sim}{g})\sum_{\lambda} e^{i(\underset{\sim}{k}_i-\underset{\sim}{k}_f)\cdot\underset{\sim}{d}_\lambda}\, T_\lambda(\underset{\sim}{k}_f, \underset{\sim}{k}_i; E) \qquad (2)$$

The vector $\underset{\sim}{d}_\lambda$ gives the position of the origin in the λth layer with respect to the origin in the surface layer. The incident and final electron wavevectors are respectively $\underset{\sim}{k}_i$ and $\underset{\sim}{k}_f$, and A is the area of the unit cell in a plane parallel to the surface. The delta function, $\delta(\underset{\sim}{k}_{f_{\shortparallel}}-\underset{\sim}{k}_{i_{\shortparallel}}-\underset{\sim}{g})$, expresses the condition for the existence of diffraction beams. The component of the outgoing beam parallel to the surface, $\underset{\sim}{k}_{f_{\shortparallel}}$, can differ from the parallel component of the incident beam, $\underset{\sim}{k}_{i_{\shortparallel}}$, only by one of the two dimensional reciprocal lattice vectors, $\underset{\sim}{g}$, of the surface. T_λ is the t-matrix for scattering of an incident electron by the λth layer in the presence of the

other layers.

The quantity $T_\lambda(\underset{\sim}{k}_f,\underset{\sim}{k}_i;E)$ can be obtained in a convenient algebraic form by means of a partial wave expansion using the conventional spherical

harmonics $Y_{lm}(\underset{\sim}{k})$, where $\underset{\sim}{k}$ is a vector whose spherical components are the angles θ and ϕ,

$$T_\lambda(\underset{\sim}{k}_f,\underset{\sim}{k}_i;E) = \sum_{lm}\sum_{l'm'} T_\lambda^{lm,l'm'}(E)\; Y^*_{lm}(\underset{\sim}{k}_f)\; Y_{l'm'}(\underset{\sim}{k}_i) \qquad (3)$$

All directional information for the incident and outgoing beams is contained in the spherical harmonics, and the matrix $T_\lambda^{lm,l'm'}(E)$ is a function only of the energy. Once this matrix is calculated, it is a simple matter to repeat the summation in equation (2) for all beams $\underset{\sim}{g}$ of interest. It is customary to replace the double index (lm) by a single index, (lm)→ L. Using this notation, equation (2) can be written

$$I_{\underset{\sim}{g}}(\underset{\sim}{k}_f,\underset{\sim}{k}_i;E)=\frac{(2\pi)^2}{A}(\underset{\sim}{k}_{f_{//}}-\underset{\sim}{k}_{i_{//}}-\underset{\sim}{g})\sum_{L,L'} Y^*_L(\underset{\sim}{k}_f)Y_{L'}(\underset{\sim}{k}_i)\left\{\sum_\lambda e^{i(\underset{\sim}{k}_i-\underset{\sim}{k}_f)\cdot\underset{\sim}{d}_\lambda}\cdot T_{\lambda(E)}^{LL'}\right\}. \qquad (4)$$

The scattering problem now reduces to calculating the matrix $T_{\lambda(E)}^{LL'}$. The first approximation made is to terminate the summations over L and L', yielding a matrix of finite dimensions. Our computer program is capable of handling up to 36x36 matrices, which corresponds to a maximum l-value of 5.

The matrix $T_\lambda^{LL'}$ can then be obtained from the equations

$$T_\lambda^{LL'} = \tau_\lambda^{LL'} + \sum_{L''}\tau_\lambda^{LL''}\sum_{\lambda'\neq\lambda}\sum_{L'''} G_{\lambda\lambda'}^{L''L'''}\; T_{\lambda'}^{L'''L'}, \text{ where} \qquad (5)$$

$$\tau_\lambda^{LL'} = t_\lambda^{LL'} + \sum_{L''} t_\lambda^{LL''} \sum_{L'''} G_{sp}^{L''L'''} \cdot \tau_\lambda^{L'''L'}, \text{ and} \tag{6}$$

$$t_\lambda^{LL'} = \delta_{\ell\ell'}\delta_{mo} \cdot \frac{i\hbar^2}{4mk} [\, e^{i\,2\delta_\ell(E)} - 1\,]. \tag{7}$$

Equation (7) is the t-matrix for the elastic scattering of an incident electron of mass m and wavevector $\underset{\sim}{k}$ from a potential characterized by a set of energy dependent phase shifts δ (E). The only conditions on the potential at this point are that it be spherically symmetrical and that neighboring potentials not overlap. Duke and Laramore[12] have shown that lattice motion can be taken into consideration at this point by renormalization of the site scattering vertices t_λ. The renormalized quantity b_λ is expressed

$$b_\lambda(\underset{\sim}{k}_f,\underset{\sim}{k}_i;E) = t_\lambda(\underset{\sim}{k}_f,\underset{\sim}{k}_i;E)\; e^{-W_\lambda(\underset{\sim}{k}_f-\underset{\sim}{k}_i)} \tag{8}$$

where $W_\lambda(\underset{\sim}{k}_f-\underset{\sim}{k}_i)$ is the Debye-Waller factor for the λth layer. If we use the Debye model for the phonon spectrum, the resultant matrix $b_\lambda^{LL'}$ is diagonal as was $t_\lambda^{LL'}$. The effect of finite temperature is thus to alter the phase shifts $\delta_\ell(E)$ appearing in equation (7). This is done internally in the computer program by expanding the exponential term in equation (8) in spherical harmonics. Note that provision is made in equation (8) for a layer dependent Debye-Waller factor, $W_\lambda(\underset{\sim}{k}_f-\underset{\sim}{k}_i)$.

Returning to equation (6), the quantity $\tau_\lambda^{LL'}$ represents the t-matrix for scattering from a single plane λ parallel to the surface. The matrix $G_{sp}^{L''L'''}$ is the subplane propagator which is calculated by a summation over

the site positions in plane λ. In order to include non zero temperature effects, the quantities $b_\lambda^{LL'}$ described above should be substituted for the $t_\lambda^{LL'}$. Equation (5) completes the definition of $T_\lambda^{LL'}$, employing $G_{\lambda\lambda'}^{L''L'''}$ as the propagator matrix for scattering from layer λ' to layer λ. Thus, $T_\lambda^{LL'}$ is composed of the scattering of a plane wave from the λth layer, $\tau_\lambda^{LL'}$, plus the contributions from all possible interplane scattering combinations ending on layer λ.

The matrix equation (6) can be inverted to yield an exact expression for τ_λ,[4]

$$\tau_\lambda = [t_\lambda^{-1} - G_{sp}]^{-1} \tag{9}$$

Equation (5) can be similarly inverted, but the summation over the total number of layers $\lambda' \neq \lambda$ leads to a matrix of impractically large dimensions. In practice, we truncate the calculation by considering only several of the outermost layers in the surface region. Satisfactory results are obtained by writing equation (5) as a perturbation expansion and iterating until the desired accuracy is obtained. Due to the inelastic damping factor which appears in the expression for the interplane propagator $G_{\lambda\lambda'}$, this convergence is rapid and reliable.

In the following sections we will systematically vary several of the input parameters mentioned in the foregoing description of the computer program. Among these are the number of phase shifts used to characterize the ion core site potential (maximum l-value), the number of outer crystal layers included in the summation (λ), the order of multiple scattering considered in the iterative solution of equation (5), and the effect of a

layer dependent Debye-Waller factor $W(\underset{\sim}{k}_f - \underset{\sim}{k}_i)$. We perform all calculations in the energy range between 40eV and 150eV. At lower energies the inner potential changes rapidly, based on free electron gas calculations, and experimental difficulties can occur in determining the precise angle of incidence of the electron beam due to small stray magnetic fields. At energies in excess of 150 eV, a larger number of phase shifts ($\ell_{max.} > 5$) must be employed to characterize the ion core potential. The penetration depth of the beam is approximately proportional to $\sqrt{E}$, giving rise to increased sampling of the bulk structure at higher energies.

II. Ion-core potentials and energy dependent phase shifts

The scattering potential at a lattice site is specified by a number of pre-calculated, energy dependent phase shifts $\delta_l(E)$. These phase shifts may be obtained at present from self-consistent APW potentials[14] or by the ab initio method of Pendry[15]. Apparently, the description of the scattering process by these two methods is of sufficient accuracy to yield qualitatively correct theoretical beam intensity-vs-incident electron energy (I-eV) curves. However, as closer agreement with experiments is sought and as surface overlayers (especially molecular overlayers) are investigated, it may be necessary to investigate these scattering potentials in more detail.

The first numerical results obtained by Duke and Tucker[5,6] were based on an s-wave approximation to the scattering amplitudes. Since that time, calculations for aluminum have appeared utilizing from three to eight phase shifts[7,9,10,12,16]. In figure (1) we plot the I-eV curve for the (100) face, 00-beam of Aluminum. The plots are for normal incidence of the electron beam, with the sample temperature at 293 K ($\Theta_D(\text{surf})=\Theta_D(\text{bulk})=426$ K). Five surface layers have been included in the calculation. Throughout this paper we employ the ion-core potential obtained from a computer program supplied by Pendry[17].

Although no experimental results exist for normally incident 00-beams, the curves thus obtained using 5 or 6 phase shifts bear a close qualitative resemblance to experimental results whose incident beam impinges at 6 degrees from the normal. A direct comparison of the incident angle dependence of the intensity patterns will be made in section V. From figure (1)

it is apparent that the I-vs-eV curves calculated using only the first two phase shifts are poor approximations to the observed intensity patterns. Furthermore the intensity scale of the lower curves compared to that of the upper curves, in which three or more phase shifts are included, shows that an almost insignificant portion of the total scattering power arises from the first two partial waves. The upper set of curves in figure (1) demonstrates a remarkable qualitative similarity between all curves which include more than two phase shifts. Tong and Rhodin have pointed out the dominance of d-wave scattering for energies in excess of 24 eV[9]. Equally striking, however, is the sharp decrease in scattered intensity upon adding the ℓ=3 phase shift to the calculation. Peak positions are altered by up to 2 eV as each additional phase shift is included. The two most intense peaks (corresponding closely to the locations of single scattering or kinematic peaks) appear to be most sensitive to this variation, whereas the two smaller multiple scattering peaks are more stable with regard to peak location.

The low scattering power of the ℓ=0 partial wave can be explained by the $(2\ell+1)$ weighting factor that appears in each term of the expansion for the scattering amplitude $f(\theta)$, even though the magnitude of the phase shift may be large. This feature will persist in all materials. The fact that inclusion of the ℓ=1 phase shift also yields such a small scattering power is partially due to the $(2\ell+1)$ factor, and partially due to the particular potential for Aluminum in which $\delta_1(E)$ passes through zero near 50 eV. In figure (1) we note that the intensity patterns stabilize when

5 to 6 phase shifts are included in the calculation. For this reason we choose to work with the first 5 phase shifts throughout this paper whenever an accurate comparison to experimental results is sought.

III. The effect of including various numbers of layers parallel to the surface in the calculation.

Due to the large inelastic damping parameter, corresponding to an attenuation length of from 4 to 10 Angstroms[5] within the crystal at low electron energies ($E \lesssim 200$ eV), the major portion of the elastic LEED scattering arises from events in the outermost layers of the sample. The computer program has been constructed so that an arbitrary number of layers may be included, and the results for Al(100) are plotted in figures (2) and (3). All these curves are calculated to tenth order diffraction between the layers, which corresponds very closely to an exact matrix inversion process.

In figure (2a) it is seen that broad peaks occur near the expected Bragg peak locations for the 2-layer calculation. Inclusion of a third layer suddenly brings out the secondary peak structure which does not change significantly in amplitude as additional layers are included in the calculation. The same general features are observed when the $\ell=3$ phase shift is added (figure 2b). Peak positions shift slightly ($\lesssim 1$ eV) with the addition of each layer.

It should not be surprising that the consideration of only three surface layers should suffice to yield a LEED pattern comparable with a more exact treatment. The interlayer spacing for the Aluminum (100) surface is 2.02 Å and the inelastic damping length is 6.4 Å at 50 eV and 7.7 Å at 100 eV for a free electron gas whose density is the same as that of the aluminum conduction electrons. Thus, the amplitude of an electron

scattered kinematically (the most favorable case) from the fourth layer is diminished by a factor of 0.15 to 0.2 compared to one scattered from the surface layer.

In section VII we will consider non-(00) beams diffracted from the same crystal surface. In order to establish the reliability of the results for these beams we include a similar calculation for the (11), and (20) beams including 2, 3 and 4 layers (see figure (3a,b)). These beams are computed for a normally incident beam on an undistorted crystal using 5 phase shifts.

It is to be expected that the addition of a third surface layer would sharpen the Bragg peaks. This is shown for a kinematical calculation in figure (4), in which no multiple scattering structure can occur. It is remarkable, however, that the secondary, or multiple scattering, structure shown in figures (2a,b) occurs suddenly with the inclusion of the third layer in the calculation.

The origin of the part of the structure attributable to multiple scattering can be identified in the 3-layer model by performing the calculation while eliminating interplane scattering between certain pairs of layers. The results of this procedure are shown in figure (5). Curve (5a) is the result of inclusion of interplane scattering between each of the three pairs of layers. Curves (5b) and (5c) are the same calculation with the elimination of scattering between layers 1 and 3 (5c), and the elimination of scattering between nearest neighbor layers (5b). The elimination of nearest neighbor layer scattering while retaining that between layers 1

and 3 preserves the structure of the secondary peak near 50 eV, whereas the reverse of this procedure does not. This behavior can only be attributed to the detailed summation of phases and amplitudes from the scattering by ion cores of one layer to a location on a different layer and will depend on the ion core potential as well as on the layer geometry and interlayer separations.

IV. Multiple scattering order and temperature effects

The iterative method used to solve equation (5) has been outlined in Section I. We can use the same method to invert equation (6) provided the scatterer is sufficiently weak[18]. This is the case for aluminum where we have compared the iterative procedure to the exact matrix inversion method. The iterative procedure is up to 20% faster in computer time and generally converges within ten iterations to a value of $\Delta \lesssim 10^{-5}$, where $\Delta = \left| |\tau^2|_{\text{inverted}} - |\tau|^2_{\text{iterated}} \right|$ and

$$\tau = \sum_L \sum_{L'} \left\{ \tau^{LL'} \; Y_L^*(\underset{\sim}{k}_f) \; Y_{L'}(\underset{\sim}{k}_i) \right\} .$$

In figure (6) we plot results for the (100) face and 00-beam of aluminum in which different interplane diffraction orders are calculated. The "matrix-inversion" results are obtained by allowing the calculation to iterate to tenth order in multiple scattering between planes. In all cases, the percentage difference between the ninth and tenth order iterations for the beam intensities is less than 0.3%. Comparison of the curves in figure (6) indicates that third order diffraction yields results that are very close to those obtained from "matrix inversion", differing by a maximum of 10% at higher energies.

The elastic force constants between the outermost surface layer and the bulk can be different from those between two bulk layers. As a result, the Debye temperature assigned to the surface layer may be quite different from the bulk value. For this reason we have calculated energy-vs-intensity

curves employing a surface Debye temperature Θ_D^{surf}=300° K and bulk value of Θ_D^{bulk}=426° K, and compared the results to a calculation involving a single $\Theta_D = \Theta_D^{bulk}$. In this paper all calculations are carried out for a crystal sample at room temperature, T = 293 K. The results are given in figure (7) for the (100) face, 00-beam of aluminum. The peak intensities are uniformly diminished due to the larger average thermal displacement of the outermost layer, but no shifts in peak positions are observed. At the present stage of theoretical accuracy there is no reason to include layer dependent Debye temperatures when working with a clean metal crystal, as the intensity ratios and the qualitative appearance of the patterns change only slightly. Separate surface values of Θ_D^{surf} should be included in the calculation of intensity curves from metals covered by overlayers of different materials since the Debye temperatures may differ significantly and the effect of this difference may vary between integral and fractional order peaks.

V. Sensitivity of calculations to the incident beam angle

It is advantageous from an experimental point of view to carry out intensity measurements with the incident electron beam normal to the crystal surface. Symmetrical non-00 beams can be compared in order to determine normal incidence to a high degree of accuracy. This procedure is desirable since small stray magnetic fields may cause the true normal direction to be different from the geometrical normal, especially at low incident electron energies. Due to the familiar geometry of the LEED apparatus, the 00-beam cannot be measured at precisely normal incidence. Common practice, as reported in the literature, is to allow the incident beam to strike the surface at an angle of 5 to 10 degrees from the normal[19,20]. The effects on the intensity pattern are shown in figure (8) for variation of the incident angle between zero and 10 degrees.

The peak intensities, especially of the high energy peaks, are significantly altered by a change in the angle of incidence of a few degrees. Measurements of the non-(00) beams may thus provide more accurate surface structure information than the 00-beam since normal incidence can be achieved experimentally to high accuracy.

VI. Inner potential and inelastic damping factor

Many body interactions between the incident electron and the electrons of the solid give rise to a complex self-energy, $\Sigma(\underset{\sim}{k},E)=\Sigma_1(\underset{\sim}{k},E)-i\,\Sigma_2(\underset{\sim}{k},E)$, where E and $\underset{\sim}{k}$ are the asymptotic energy and propagation vector of the incident electron far outside the crystal. The real part of $\Sigma(\underset{\sim}{k},E)$ represents the "inner potential" familiar in LEED studies, and the imaginary part gives rise to inelastic damping of the incident beam. There exists as yet no calculation for $\Sigma(\underset{\sim}{k},E)$ involving a realistic crystal lattice. In the absence of such a calculation, three kinds of approximations have found frequent use:

1) Constant elastic electron mean free path. The real part of the self energy, $\Sigma_1(E)$, is assigned a constant value equal to the energy difference between the APW muffin tin zero and the vacuum level[12]. The imaginary part of the self energy, $\Sigma_2(E)$, is an energy dependent function obtained by assuming the elastic electron mean free path to be a constant over the LEED energy range. This constant is assigned a value that yields peak widths in accord with experimental observations. Laramore and Duke[12] use this method and obtain

$$\Sigma_2(E) = -\left(\frac{\hbar^2}{m\lambda_{ee}}\right)\left(\frac{2m}{h^2}\,[E-\Sigma_1]\right)^{1/2}, \qquad (10)$$

where λ_{ee} is twice the electron mean free path. This mean free path yields acceptable peak widths in LEED calculations for values of $\frac{\lambda_{ee}}{2}$ from 4 to 10 Angstroms.

2) The optical model potential. In this model the complex self energy $\Sigma(\underset{\sim}{k},E)$ is taken to be independent of $\underset{\sim}{k}$ and E[7]. The real part, $\Sigma_1(\underset{\sim}{k},E)$, is either assigned the value of the APW muffin tin zero, or determined empirically by shifting the calculated intensity pattern to achieve a best fit to experiment. The imaginary part $\Sigma_2(\underset{\sim}{k},E)$ is assigned a constant value equal to that derived from a many body calculation of a free electron gas whose density is equal to the conduction band electron density of the solid. The inelastic damping length λ_{ee} varies slowly with energy and is in the 4A to 8A range for incident electron energies in the LEED range for typical metals.

3) The free electron gas self energy. A computation has been performed by Lundqvist[21] in which the energy dependent real and imaginary parts of Σ are calculated for a uniform electron gas. This approach has been used by Tong and Rhodin[9] to calculate aluminum (100) intensity patterns. It is not presently known how closely the free electron gas model approximates the self energy of a real crystal, but it has proved useful as a model for that problem.

Calculations available in the literature have used the APW potential of Snow[14] with the optical model self energy, or the Pendry potential[15] with the free electron gas self energy. Either approach yields calculated intensity curves in acceptable qualitative agreement with experiment. In order to obtain better quantitative agreement it is instructive to compare the results of both approximations to the self energy with the same crystal potential. The results of doing this are plotted in figure (9) for aluminum,

using Pendry's potential including 5 phase shifts.

The two approximations do not necessarily represent extremes between which the results for a real crystal must lie, but they do provide an upper limit on the confidence we are justified in placing in a given calculation. Until convincing reasons can be put forth for using a specific form for the energy dependence of the self energy in a real crystal, we are forced to regard skeptically claims that peak positions can be calculated to an accuracy of less than 3 eV.

VII. Sensitivity of calculations to changes in the position of the surface layer

The foregoing sections have been devoted to a methodical consideration of the computational errors that can be introduced into a LEED calculation with the variation of the numerous input parameters. These parameters fall into two general types. The first type are those parameters which cause the truncation of the calculation at a specified level of accuracy. A compromise must be made between increasing accuracy and rapidly increasing computer time and memory requirements. Three such parameters are the number of phase shifts used to characterize the ion core potential, the number of layers over which the lattice summation is made, and the order of multiple scattering involved. It is necessary to establish the probable accuracy of a calculation truncated in various manners in order to obtain an optimal set of parameters that yield results within acceptable error limits. In previous sections of this paper we have shown that for the (100) surface of aluminum acceptable peak positions and amplitudes can be obtained by including 5 phase shifts, three layers parallel to the surface and nine or more iterations in the multiple scattering summation.

The second type of parameter involved reflects our lack of detailed knowledge of the system. Phase shifts characterizing the ion core scattering can be calculated from a variety of approximations, each involving a different set of physical assumptions. It is necessary to learn which sets of assumptions lead to results that are sufficiently accurate for the purpose of surface structure analysis. The Pendry ion core potential[15] and the APW

potential of Snow [14] yield qualitatively correct LEED structure curves whereas an atomic potential does not. A comparison will be made in figure (10c). Another such parameter is the layer dependence of the Debye temperature discussed in section V.

Once this has been accomplished, we can turn to the central problem of surface structure calculations; namely, the sensitivity of computed intensity patterns to variations in the surface geometry. We have used the non reconstructed (100) face of aluminum to illustrate the effects of lateral and perpendicular displacement of the outermost crystal layer.

The effect of varying the outer layer spacing ±2% from the bulk value is plotted in figure (10a) in which the inner potential is taken as a constant throughout the energy range and determined by shifting the resulting curves to obtain a best fit to the experimental curve. The same results are plotted in figure (10b) using the Lundqvist free electron gas self energy approximation[21]. The theoretical curves in the latter case are shifted by the aluminum (100) work function of 4.2 eV[22]. For further comparison, the results of a second order perturbation calculation of Tong and Rhodin[9], and that of Jepsen, Marcus and Jona[7] using Snow's APW potential with 8 phase shifts are plotted in figure (10c). The results of a calculation using the atomic phase shifts of Fink and Yates[23] are also included.

Examination of figures (10a) and (10b) show that a change of ±2% in the perpendicular layer spacing of the outermost layer is sufficient to shift the peaks from 1 to 4 eV. The calculations are not sufficiently unambiguous, however, to allow us to state with certainty a value for the outer

layer spacing from an analysis of the 00-beam alone. This is true for three reasons; first, it is not certain how accurately the Pendry ion core phase shifts approximate the actual ion core scattering in a solid. It is clear that the Pendry calculation and those using APW potentials give good qualitative results that are not obtainable from a simple atomic potential, figure (10c), but the quantitative accuracy of the resulting peak positions is not known. Secondly, use of two different models for the inner potential (see section VI) has been seen to cause an uncertainty in peak positions by up to 3 eV. Thirdly, the calculated intensity curves have been shown to be quite sensitive to the incident angle θ (section V), and at non-normal beam incidence the peak intensities and positions can be considerably altered by an error of $\Delta\theta=\pm 2°$.

The third of these sources of error can be eliminated by working at normal incidence with non specular beams. Results are plotted in figures (11) and (12) for the 11-beam and the 20-beam. Due to the shifts of several eV between the free electron gas energy renormalization and that of the optical model potential (see section VI) we have plotted beam intensity curves using both approximations, and have included the experimental curves for comparison. For both beams considered, the qualitative agreement between theory and experiment is good for a surface layer having the same interlayer spacing as in the bulk. Alterations in the spacing from +5% to -2% of the bulk interlayer spacing cause shifts in peak positions and amplitudes and secondary peaks may be transformed into shoulders or vice versa. Use of the optical model potential with its constant value for the inner potential

moves the low energy peaks to a relatively higher energy than when the free electron gas self energy is employed. A somewhat better qualitative fit results from using a constant value for the self energy but this is achieved at the expense of adding another adjustable parameter. In summary, a surface layer spaced within ~5% of the bulk interlayer spacing yields an acceptable LEED intensity pattern for both the 11- and 20-beams on the (100) surface of aluminum.

If the surface layer were to be displaced slightly in a direction parallel to the surface it would be expected to cause a change in some or all of the LEED beam intensity curves. Such a change shows up in the calculation in two places; first, the interplane propagator matrix of equation (5) is changed in a complicated way since the horizontal spacings between all atomic positions of the surface layer with respect to the bulk layers are modified. Secondly, the phase factor $e^{i(\underset{\sim}{k}_i - \underset{\sim}{k}_f)\cdot \underset{\sim}{d}_\lambda}$ appearing in the summation of equation (2) may be of importance if the small horizontal displacement changes the argument in the exponential. For small displacements, figures (13) and (14) demonstrate that the effect of the phase factor is predominant. The displacement of the surface layer of 0.2 Å in the x-direction causes little distortion of the 00- and 11-beam LEED intensity patterns since the phase factor is either unchanged or very slightly changed. In the case of the 20-beam, however, the vector $(\underset{\sim}{k}_{i_{\shortparallel}} - \underset{\sim}{k}_{f_{\shortparallel}})$ and $\Delta d_{\lambda_{\shortparallel}}$ are collinear and the change in the phase factor causes a significant alteration of the intensity curve. The sensitivity of certain non

00-beams to small displacements in different directions parallel to the surface should be helpful in determining the surface structure of overlayers and the positions of atoms in reconstructed surfaces.

ACKNOWLEDGEMENTS

This work was supported by the U. S. Atomic Energy Commission.

We are grateful to Dr. J. B. Pendry for supplying the computer program used to calculate the ion core phase shifts.

REFERENCES

1. J. B. Pendry, J. Phys. (Sol. St. Phys.) 2, 2273, 2283 (1969).
2. G. Capart, Surf. Sci. 26, 429 (1971).
3. J. A. Strozier, Jr. and R. O. Jones, Phys. Rev. B3, 3228 (1971).
4. J. L. Beeby, J. Phys. (Proc. Phys. Soc.) [2], 1, 82 (1968).
5. C. B. Duke and C. W. Tucker, Jr., Surf. Sci. 15, 231 (1969).
6. C. B. Duke, J. R. Anderson and C. W. Tucker, Jr., Surf. Sci. 19, 117 (1970).
7. D. W. Jepsen, P. M. Marcus and F. Jona:
   Phys. Rev. Lett. 26, 1365 (1971)
   Phys. Rev. B5, 3933 (1972).
8. D. W. Jepsen and P. M. Marcus, Computational Methods in Band Theory (Plenum, New York, 1971) p. 416.
9. S. Y. Tong and T. N. Rhodin, Phys. Rev. Lett. 26, 711 (1971).
10. R. H. Tait, S. Y. Tong and T. N. Rhodin, Phys. Rev. Lett. 28, 553 (1972).
11. J. B. Pendry, Phys. Rev. Lett. 27, 856 (1971).
12. G. E. Laramore and C. B. Duke, Phys. Rev. B5, 267 (1972).
13. G. E. Laramore and C. B. Duke, Phys. Rev. B2, 4783 (1970).
14. E. C. Snow:
   Phys. Rev. 158, 683 (1967).
   Phys. Rev. 171, 785 (1968).

15. J. B. Pendry, J. Phys. (Sol. St. Phys.) 4, 2501 (1971).

16. G. E. Laramore, C. B. Duke, A. Bagchi and A. B. Kunz, Phys. Rev. B4, 2058 (1971).

17. J. B. Pendry (private communication).

18. J. B. Pendry, J. Phys. (Sol. St. Phys.) 4, 3095 (1971).

19. F. Jona, IBM Journ. of Res. and Dev. 14 (4), July 1970.

20. H. H. Farrell and G. A. Somorjai, Phys. Rev. 182, 751 (1969).

21. B. I. Lundqvist, Phys. Stat. Sol. 32, 273 (1969).

22. N. D. Lang and W. Kohn, Phys. Rev. B3, 1215 (1971).

23. M. Fink and A. C. Yates, Technical Report No. 88, Electronics Research Center, University of Texas at Austin (1970).

FIGURE CAPTIONS

Figure 1. Calculated 00-beam intensity-vs-incident electron energy for a normally incident beam including the five outermost layers. The lower two curves are computed using Pendry's ion-core potential with one and two phase shifts. The upper curves are computed including three to six phase shifts. The intensity scale of the lower curves is ten times that of the upper curves. The labelled ℓ_{max}-values refer to the largest angular momentum quantum number whose phase shift, $\delta_{\ell_{max}}(E)$, appears in the summation.

Figure 2a. Calculated 00-beam intensity-vs-incident electron energy for a normally incident beam including the two to five outermost layers in the computation. Three phase shifts ($\ell_{max} = 2$) are used for all four curves.

Figure 2b. Calculated 00-beam intensity-vs-incident electron energy for a normally incident beam including the two to five outermost layers in the computation. Four phase shifts ($\ell_{max} = 3$) are used for all four curves.

Figure 3. Calculated beam intensity for a normally incident beam as a function of incident electron energy, comparing results of including 2, 3 and 4 layers in the computation. Five phase shifts ($\ell_{max} = 4$) are used in these calculations. a) 11-beam, b) 20-beam.

Figure 4. Single scattering (kinematic) intensity-vs.-incident electron energy curves showing the increase in sharpness of the "Bragg" peaks as an increasing number of crystal layers are included in the calculation.

Figure 5. Three layer model of the crystal surface in which a) all multiple scattering is included, b) scattering between nearest neighbor layers are eliminated, and c) scattering only between nearest neighbor layers are retained.

Figure 6. Intensity curves for the 00-beam as a function of incident electron energy calculated with three layers and five phase shifts. The single scattering (kinematic) intensity curve is compared to curves obtained from a dynamic calculation with double diffraction, triple diffraction and the "matrix inversion" result.

Figure 7. The effect of a surface Debye temperature $\theta_D^S = 300°$ K on the 00-beam intensity curves is shown by the dashed and dotted lines. A total of four layers is used, and the three underlying layers are assigned a bulk Debye temperature of $\theta_D^B = 426°$ K. The solid curves are calculated for comparison, with all four layers assigned the bulk Debye temperature of 426° K. The two sets of curves include results of calculations made with three and four phase shifts at normal incidence.

Figure 8. The effect of varying the incident beam angle from normal incidence (θ= 0°) to 10° on the 00-beam I-vs-eV curves is plotted. Five phase shifts and three layers have been included in the calculations. The azimuthal angle is ϕ=45° with respect to the x-axis.

Figure 9. The 00-beam I-vs-eV curves plotted here utilize the same Pendry ion-core potential characterized by five phase shifts and three surface layers. The solid curve is plotted using the real part of the self-energy from Lundqvist's free electron gas calculation, shifted by the work function of 4.2 eV. The dashed curve is the same calculation except that the real part of the self-energy plus the work function is an empirically determined constant value of 11 eV. These curves illustrate the uncertainty in peak positions between these two models for the inner potential.

Figure 10a. The 00-beam intensity curve is calculated using five phase shifts and three layers. A constant inner potential correction is determined by shifting the curves until a best fit to the experimental data is achieved. The outer layer spacing is contracted and expanded 2% of the bulk spacing.

Figure 10b. I-vs-eV curves obtained from the same calculations are plotted using the Lundqvist free electron gas approximation for the inner potential. These curves are plotted with a 4.2 eV work function correction and no empirical fit is made to the experimental results.

Figure 10c. The experimental I-vs-eV curves for the 00-beam are compared with those obtained by various computations. The incident beam angles, Θ and ϕ, are indicated for each calculation.

Figure 11. Effect of varying the interplane spacing of the surface layer. The 11-beam intensity is calculated using the Lundqvist free electron gas approximation for the inner potential (curves B), and using an empirically determined constant value for the inner potential (curves C). These calculations are compared to the experimental result of Jona (curve A). Variations in the surface layer separation are expressed in percent of the bulk interlayer spacing (2.02 Å).

Figure 12. The 20-beam intensity is calculated using the Lundqvist free electron gas approximation for the inner potential (curves B) and using an empirically determined constant value for the inner potential (curves C). These calculations are compared to the experimental result of Jona (curve A). Variations in the surface layer separation are expressed in percent of the bulk interlayer spacing (2.02 Å).

Figure 13. The effect of a horizontal displacement of the surface layer by 0.2 Å in the x-direction on the I-vs- eV curve for the (00) beam is plotted as the dashed curve. The solid curve represents the calculation for the undistorted crystal. Four phase shifts and three crystal layers are included.

Figure 14. The effects of a horizontal displacement of the surface layer by 0.2 Å in the x-direction is plotted as a dashed curve for the 11- and 20-beams. The solid curve represents the calculation for the undistorted crystal. Four phase shifts and three crystal layers are included.

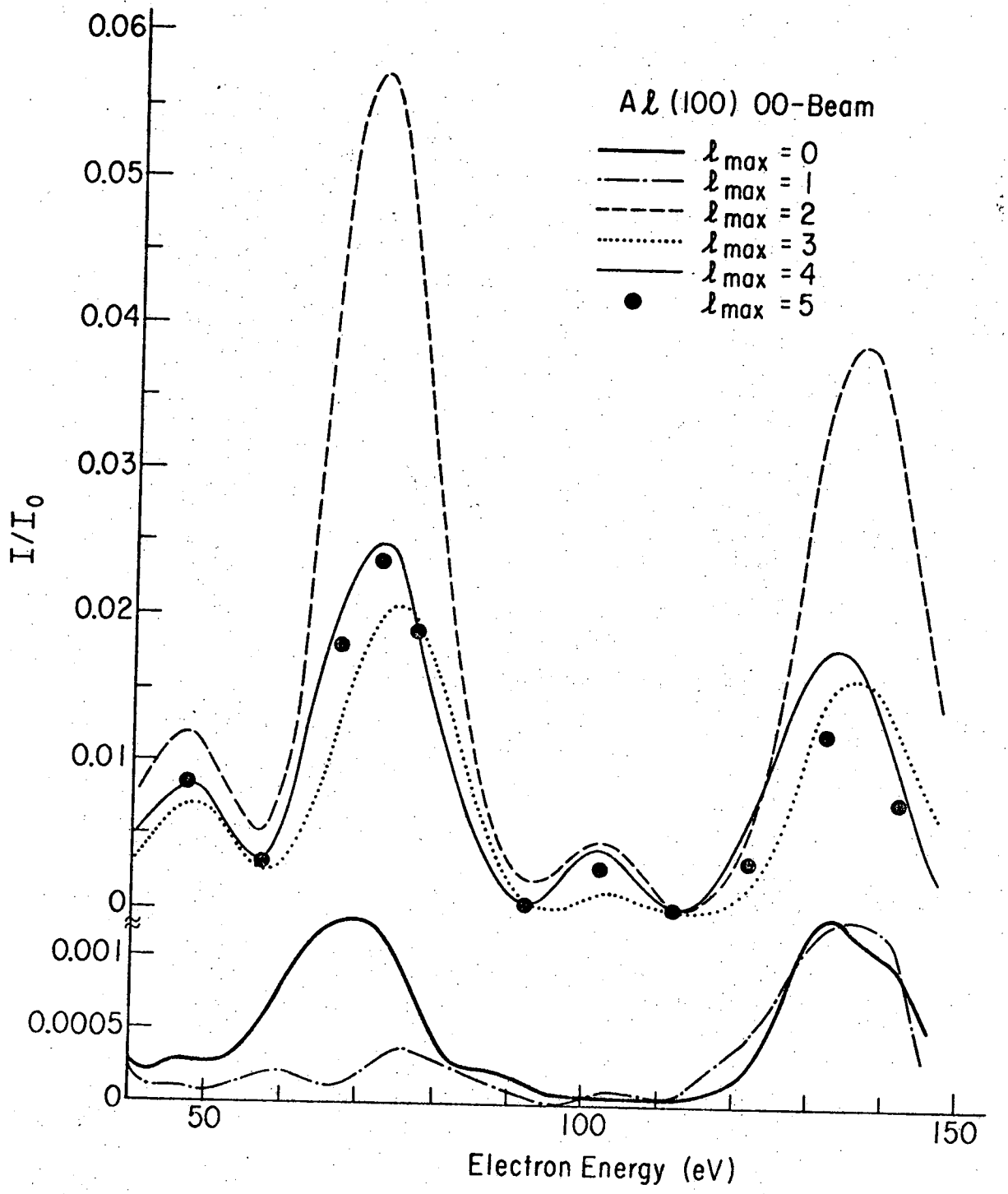
Al (100) 00-Beam
ℓmax = 0
ℓmax = 1
ℓmax = 2
ℓmax = 3
ℓmax = 4
ℓmax = 5
I/I0
0.06
0.05
0.04
0.03
0.02
0.01
0
0.001
0.0005
0
50
100
150
Electron Energy (eV)
XBL727-6570

Fig. 1

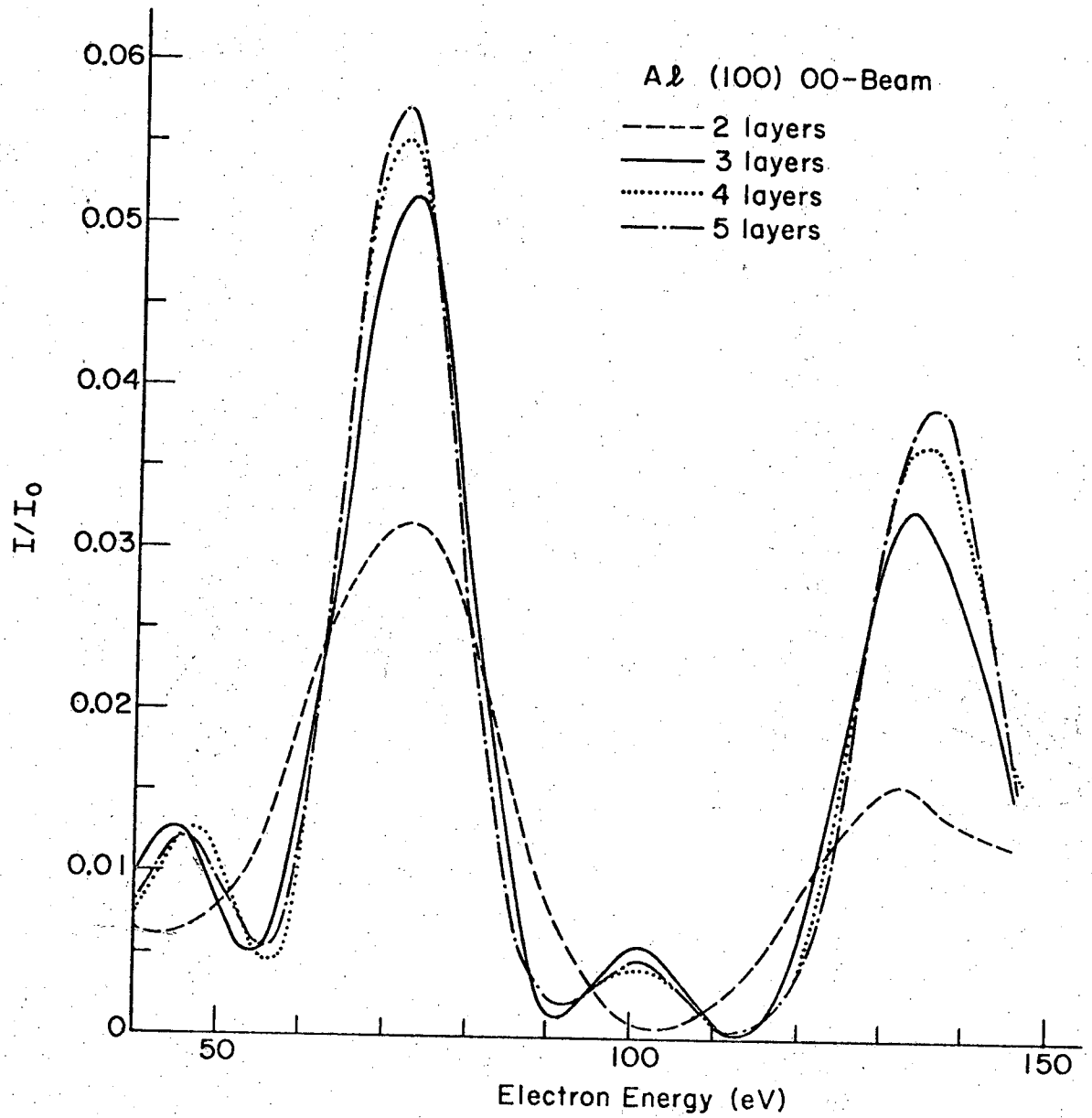
Al (100) 00-Beam
2 layers
3 layers
4 layers
5 layers
0.06
0.05
0.04
0.03
0.02
0.01
0
I/I₀
50
100
150
Electron Energy (eV)
XBL727-6571

Fig. 2a

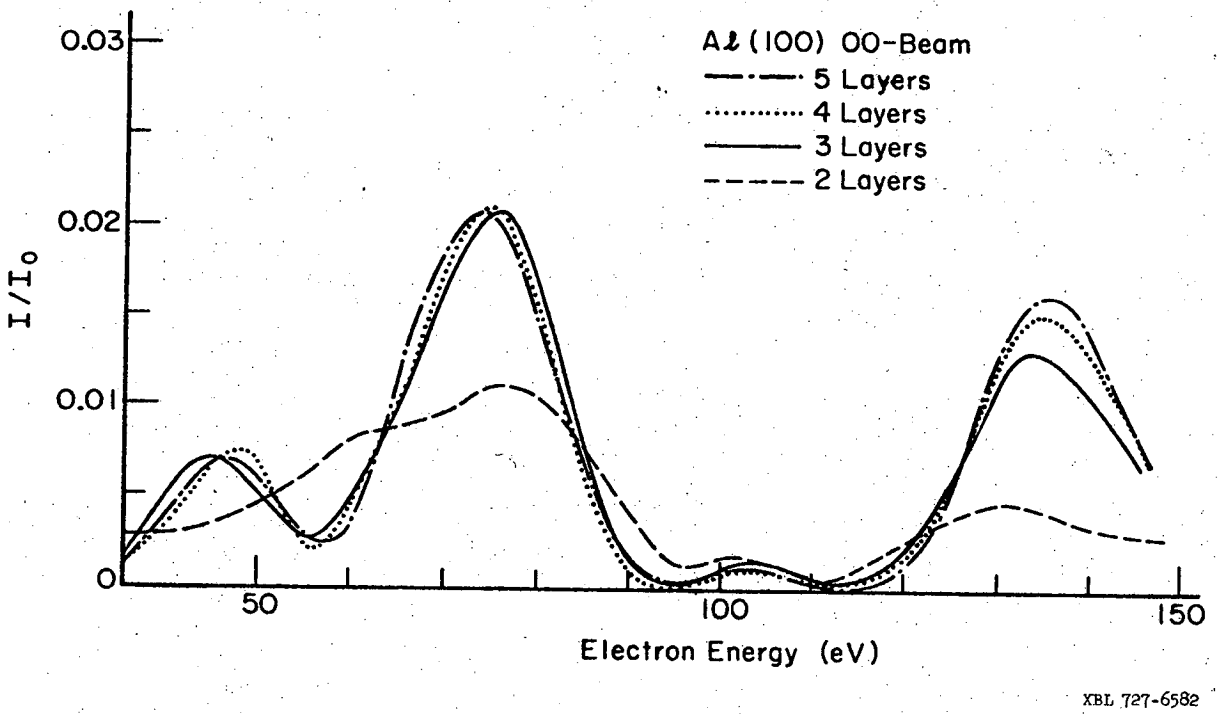
Aℓ (100) 00-Beam
5 Layers
4 Layers
3 Layers
2 Layers
0.03
0.02
0.01
0
I/I₀
50
100
150
Electron Energy (eV)
XBL 727-6582

Fig. 2b

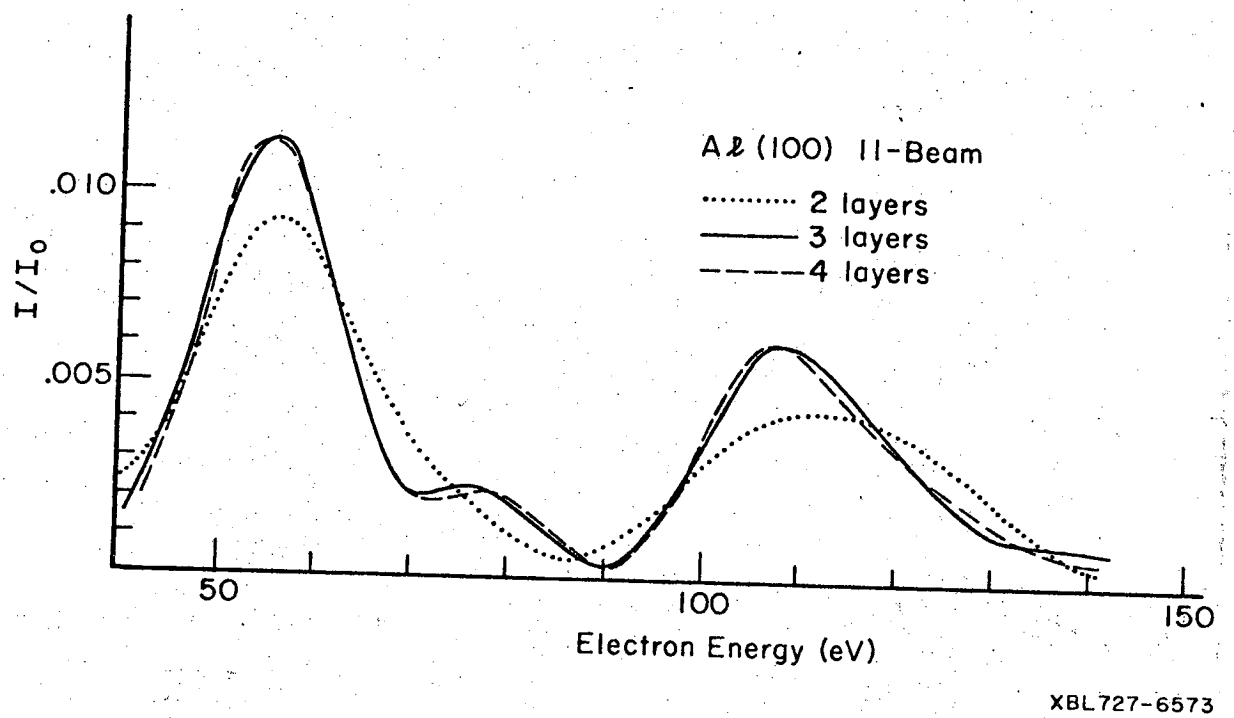
Aℓ (100) 11-Beam
2 layers
3 layers
4 layers
I/I₀
.010
.005
50
100
150
Electron Energy (eV)
XBL727-6573

Fig. 3a

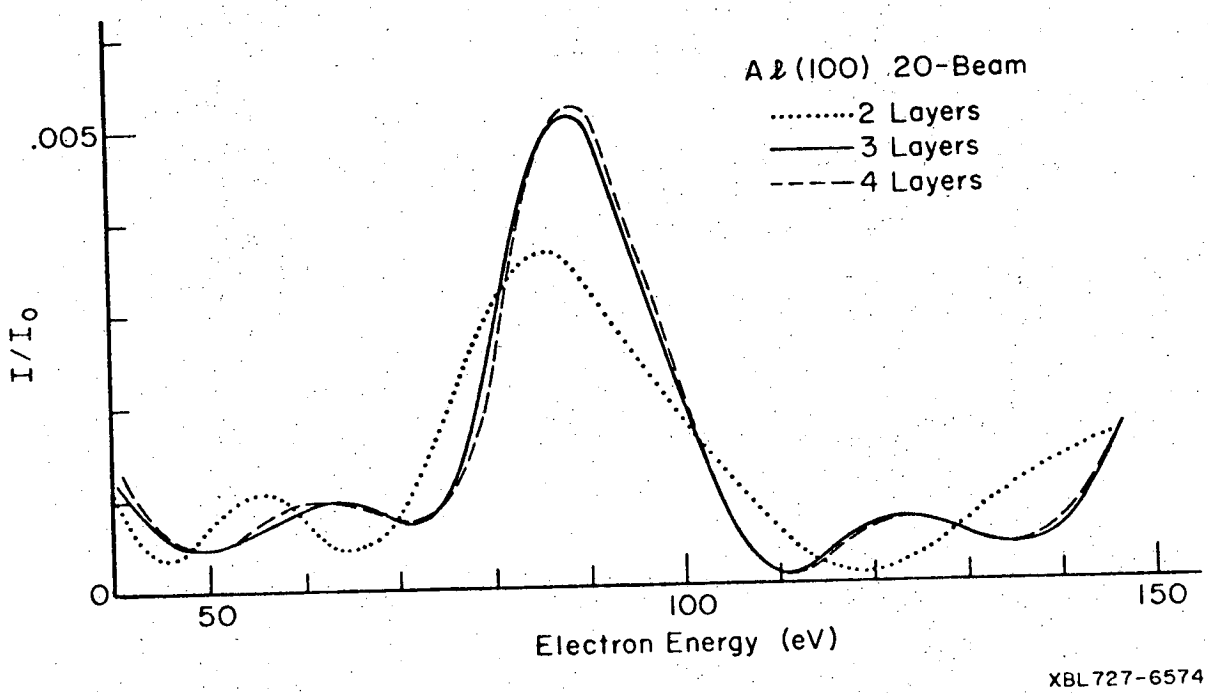
Al (100) 20-Beam
2 Layers
3 Layers
4 Layers
.005
0
I/I₀
50
100
150
Electron Energy (eV)
XBL727-6574

Fig. 3b

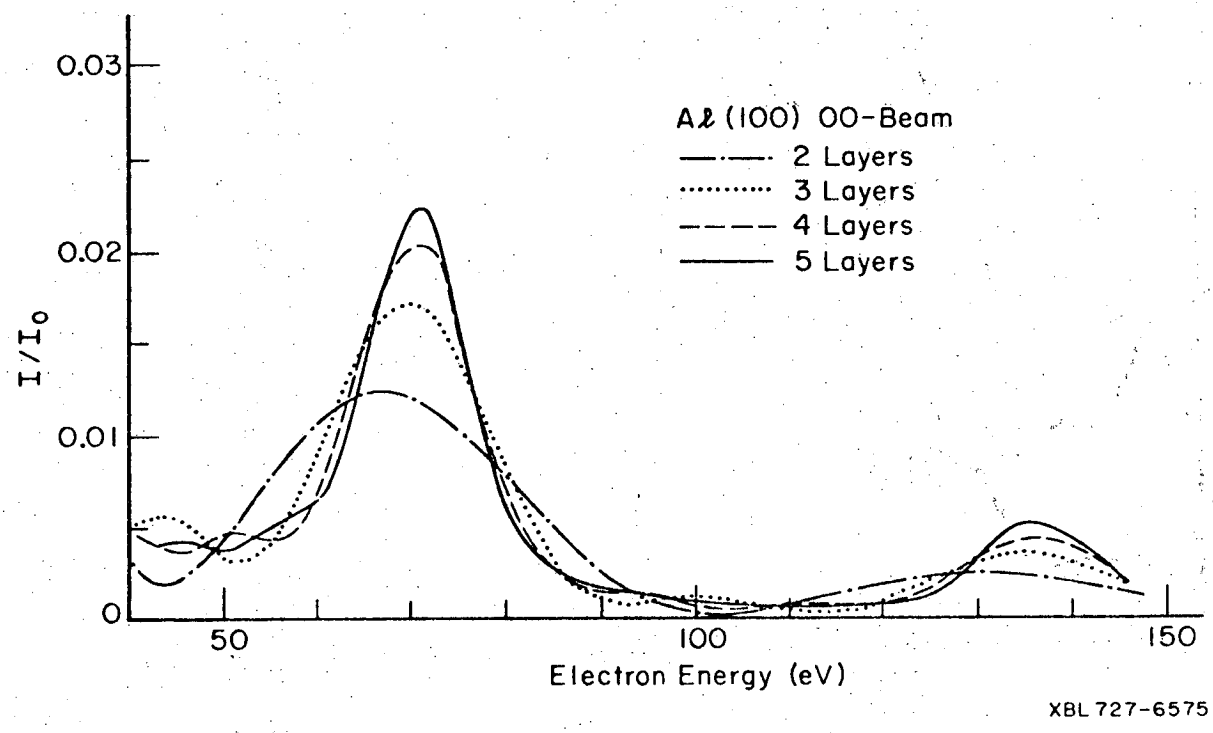
0.03
0.02
0.01
0
I/I₀
Aℓ (100) 00-Beam
2 Layers
3 Layers
4 Layers
5 Layers
50
100
150
Electron Energy (eV)
XBL 727-6575

Fig. 4

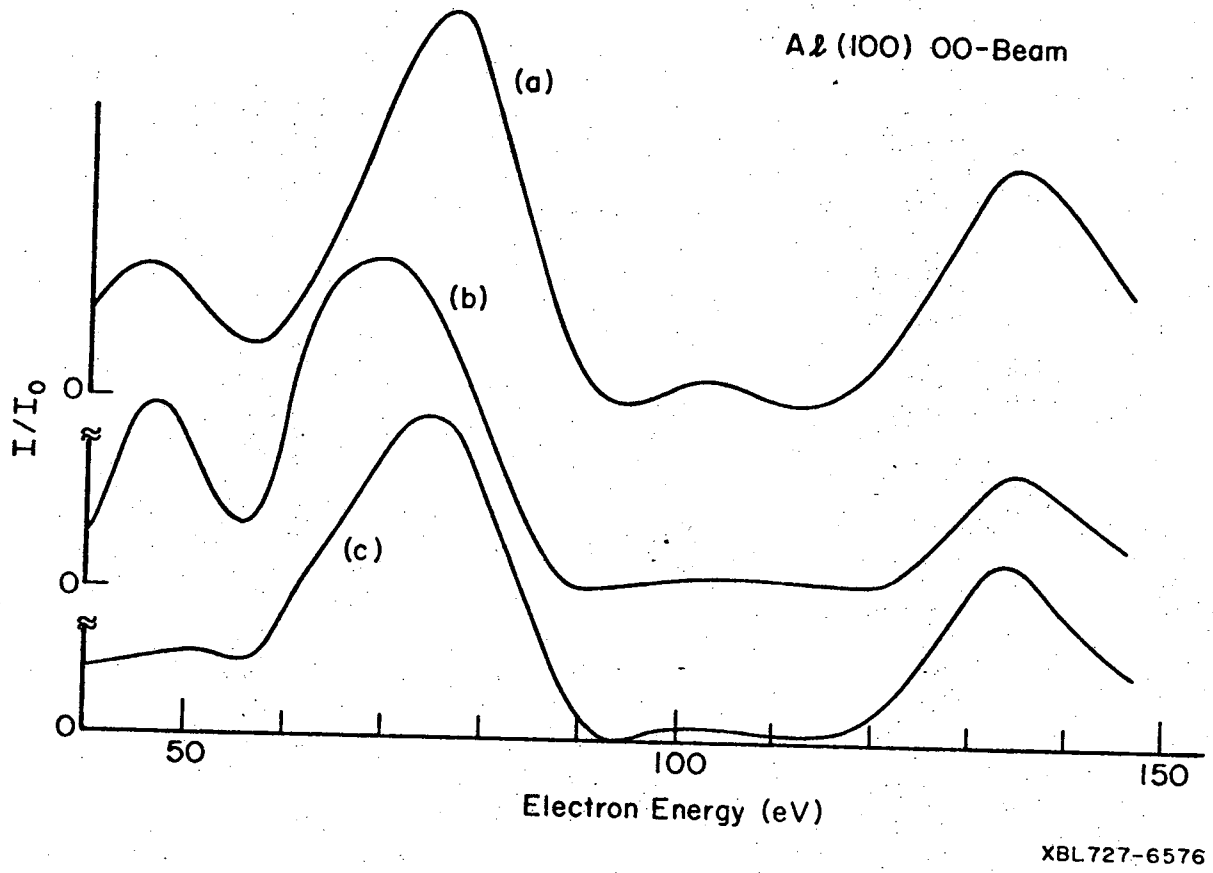
Al (100) 00-Beam
(a)
(b)
(c)
I/I0
0
0
0
50
100
150
Electron Energy (eV)
XBL727-6576

Fig. 5

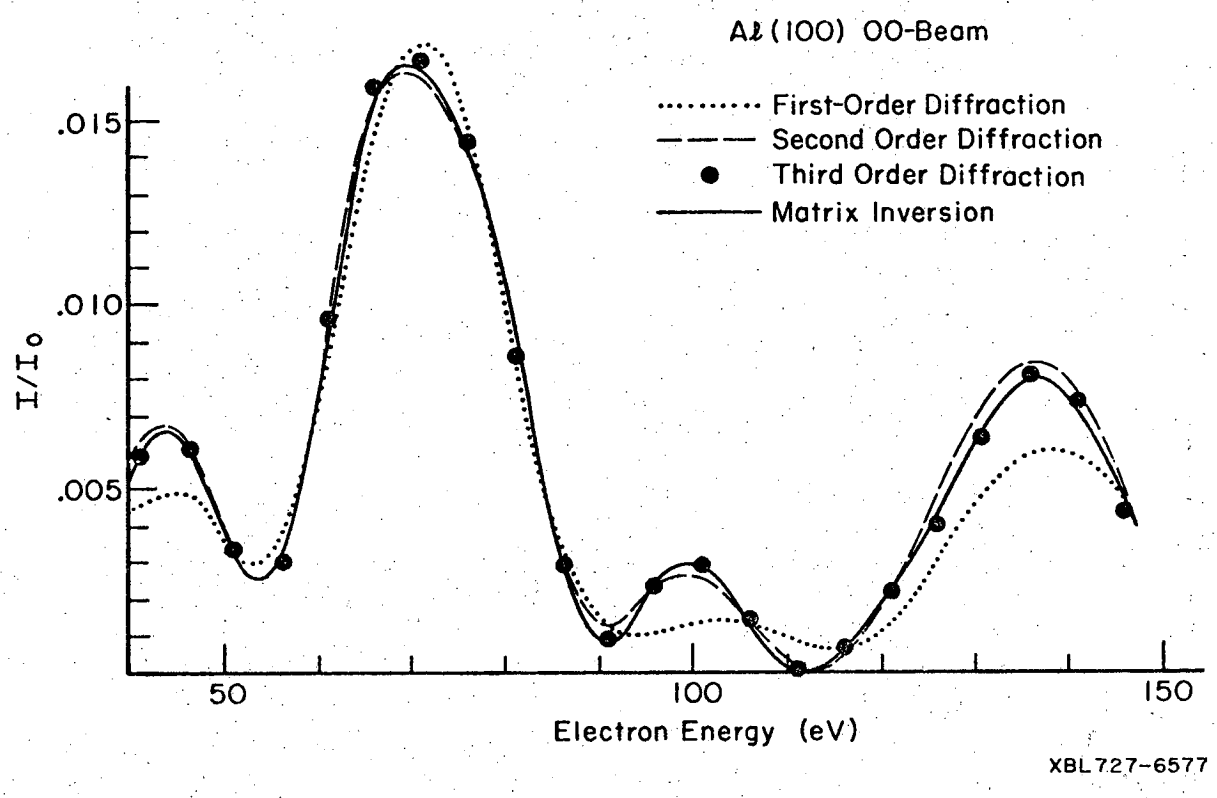

Fig. 6

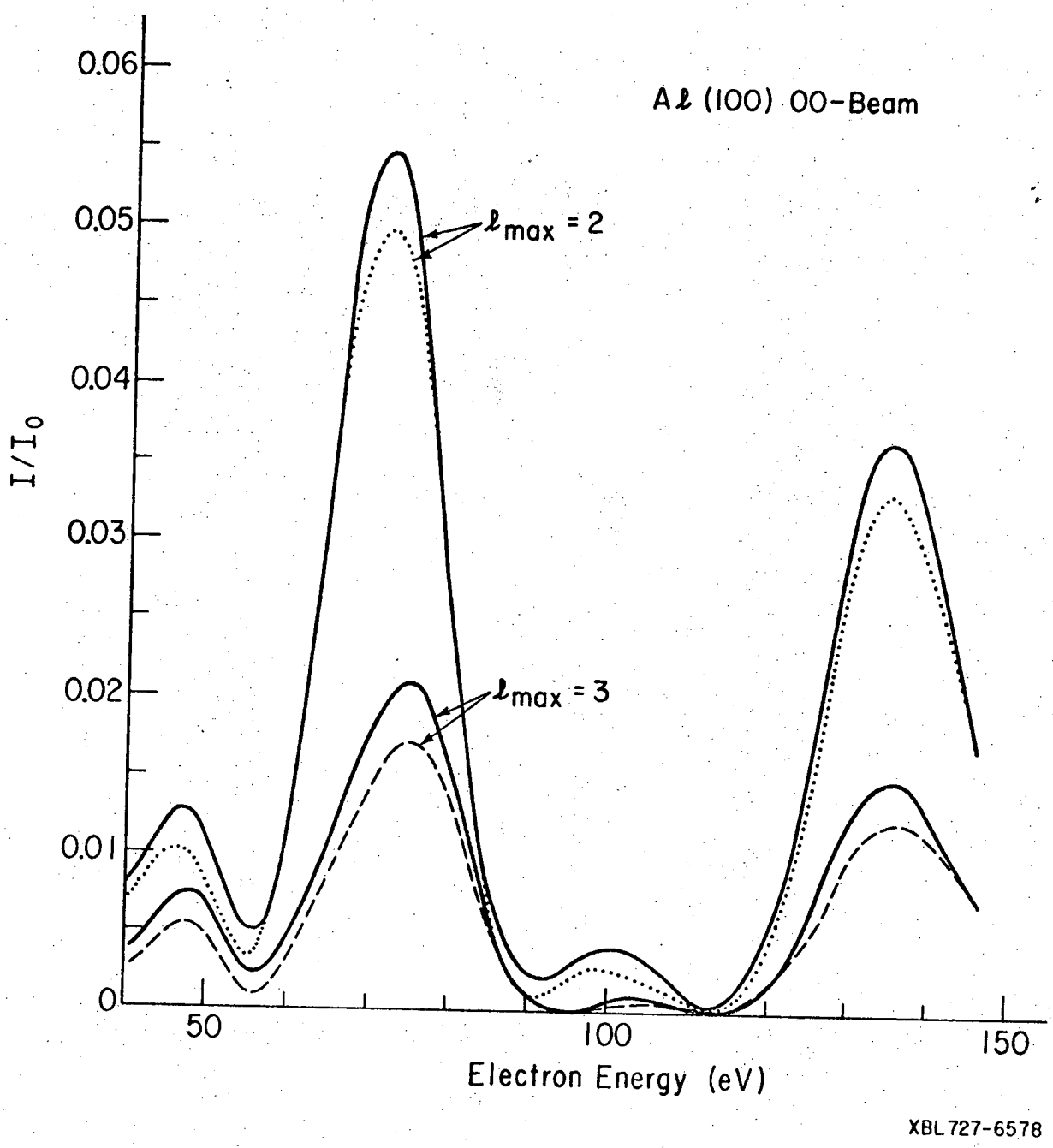
Al (100) 00-Beam
$\ell_{max} = 2$
$\ell_{max} = 3$
0.06
0.05
0.04
0.03
0.02
0.01
0
I/I_0
50
100
150
Electron Energy (eV)
XBL727-6578

Fig. 7

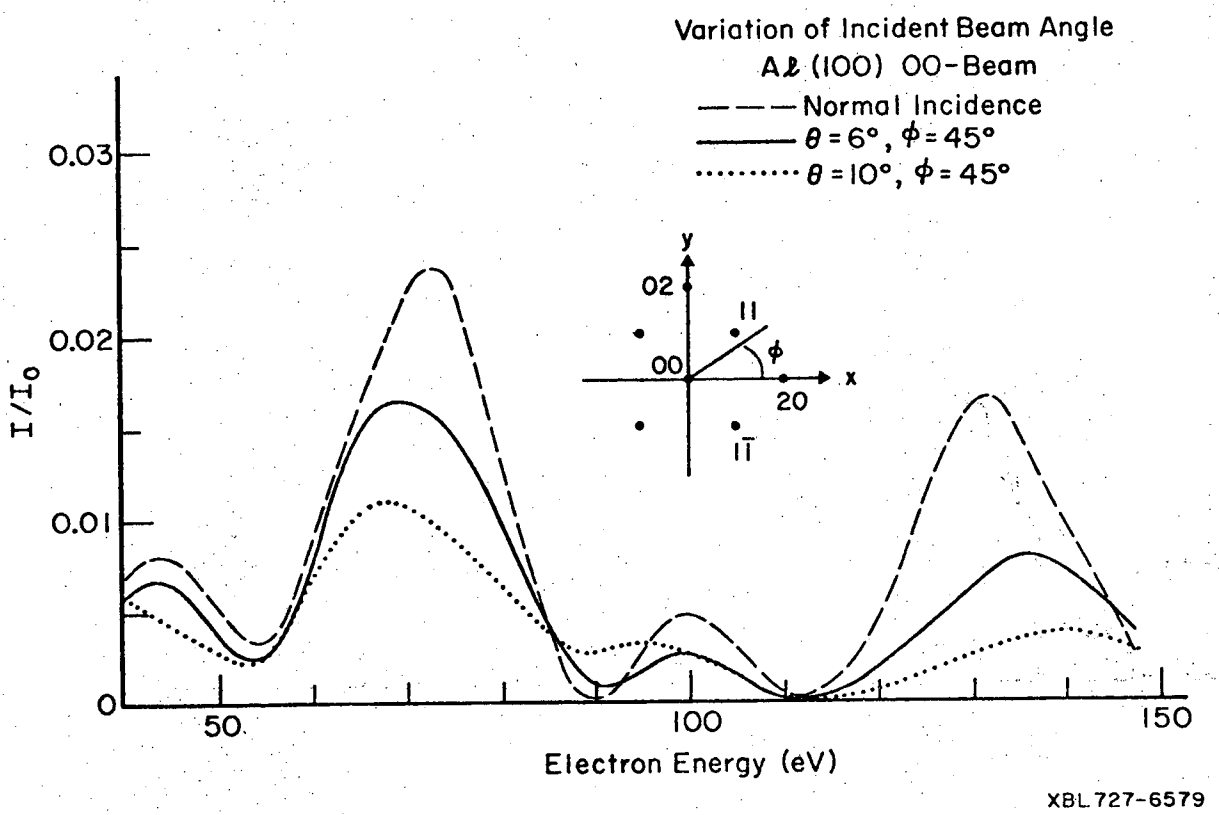

Fig. 8

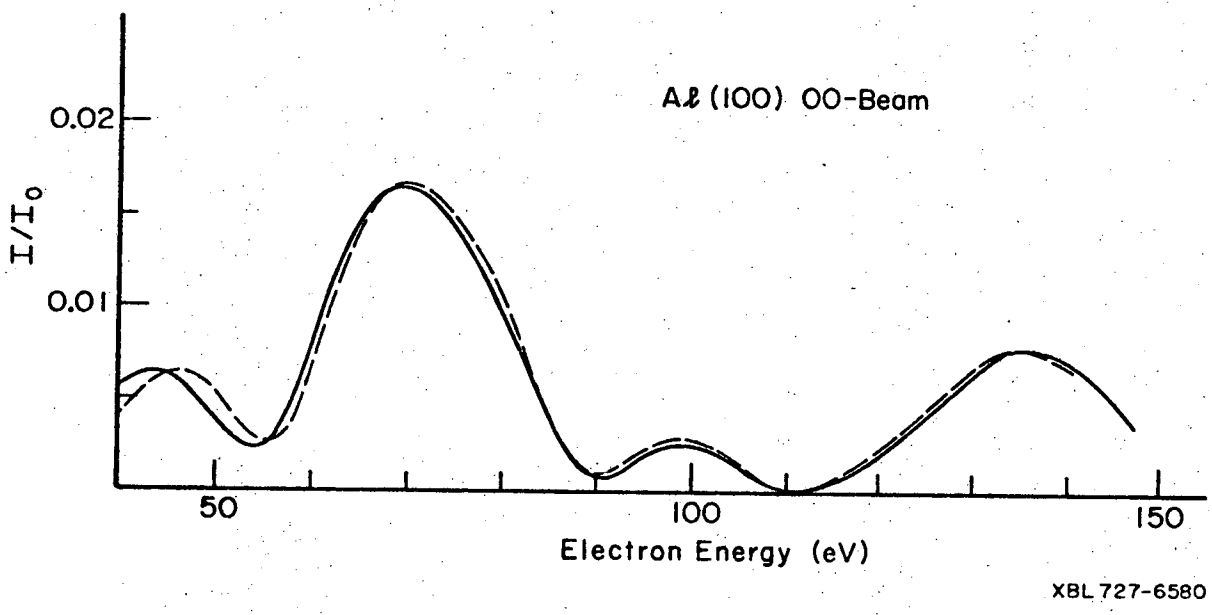
Aℓ (100) 00-Beam
0.02
0.01
I/I0
50
100
150
Electron Energy (eV)
XBL 727-6580

Fig. 9

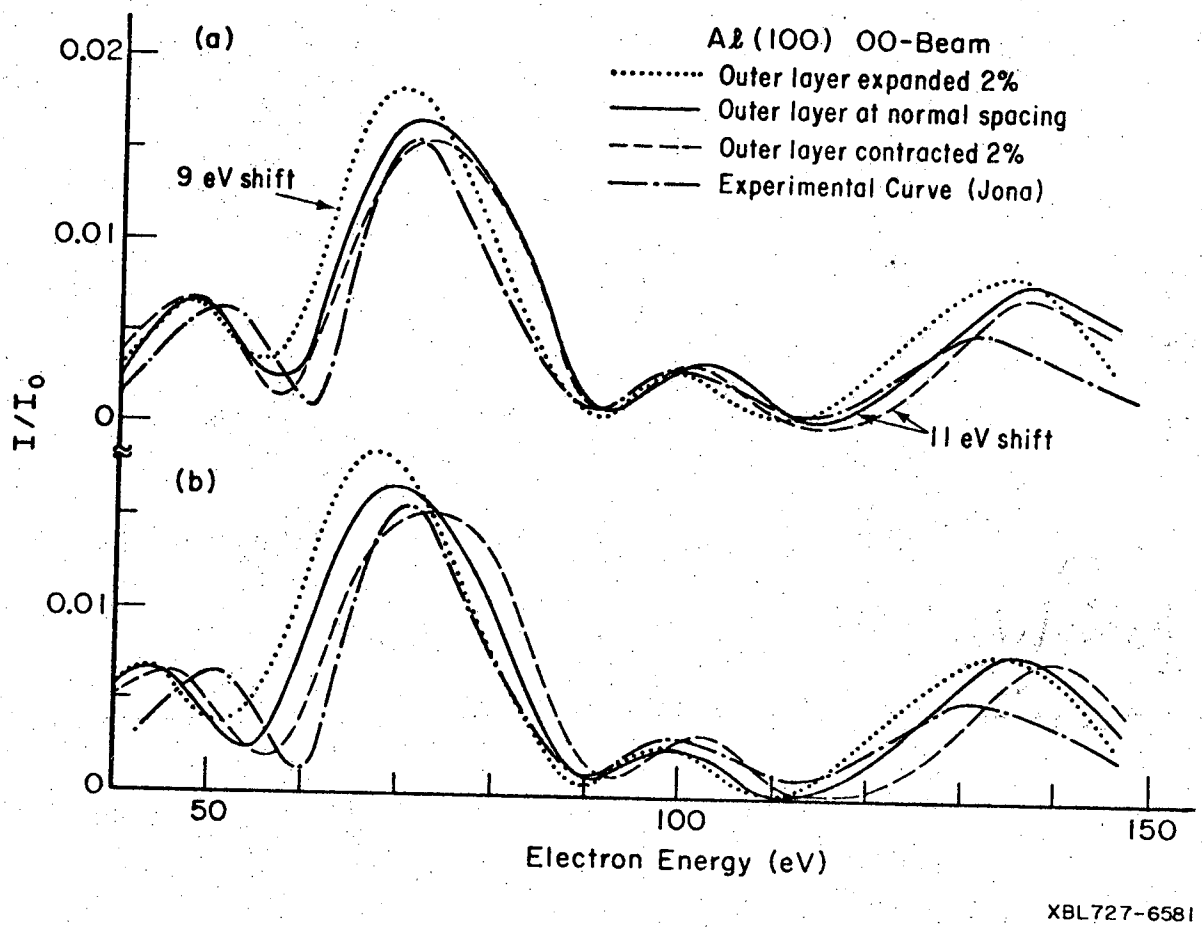

Fig. 10a and b

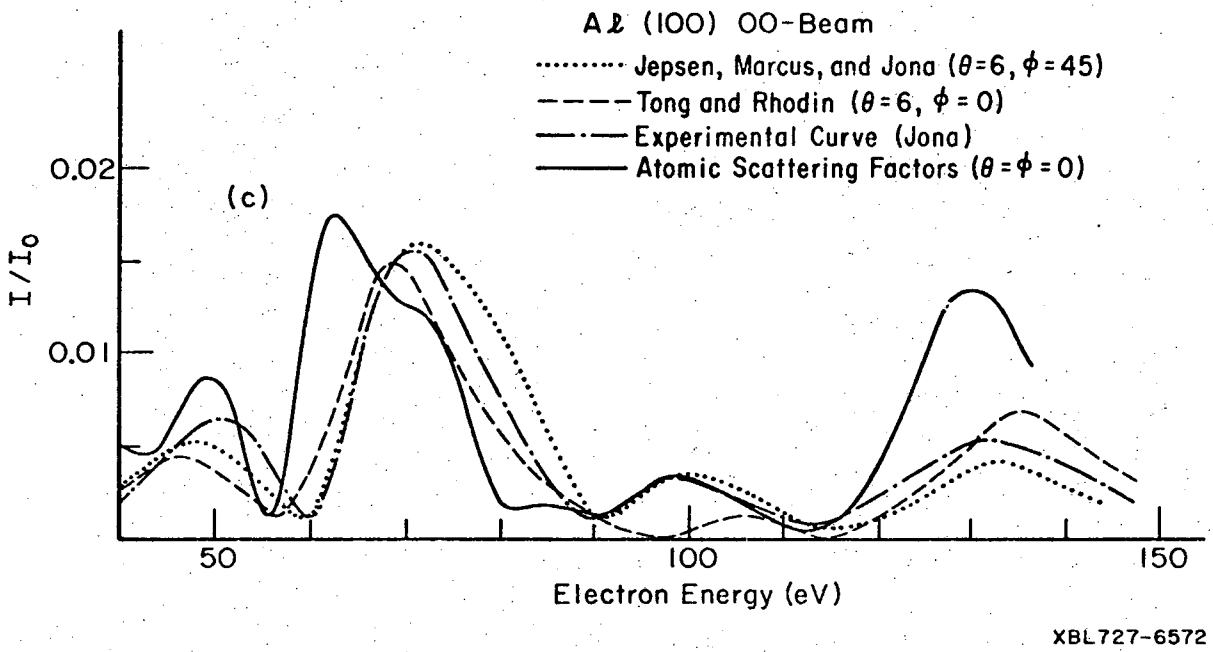
Al (100) 00-Beam
Jepsen, Marcus, and Jona (θ=6, φ=45)
Tong and Rhodin (θ=6, φ=0)
Experimental Curve (Jona)
Atomic Scattering Factors (θ=φ=0)
(c)
0.02
0.01
I/I0
50
100
150
Electron Energy (eV)
XBL727-6572

Fig. 10c

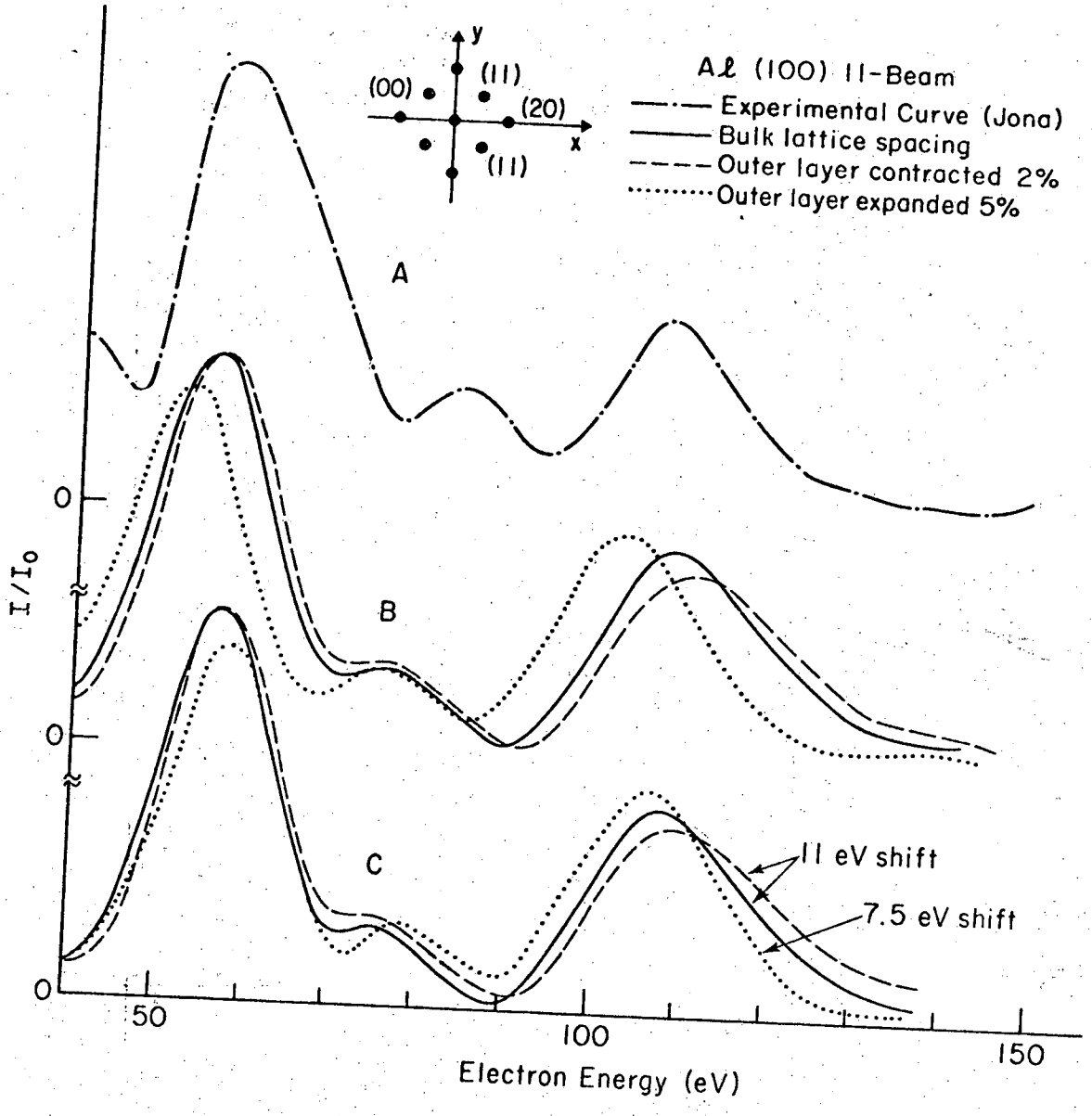
Al (100) 11-Beam
Experimental Curve (Jona)
Bulk lattice spacing
Outer layer contracted 2%
Outer layer expanded 5%
y
x
(00)
(11)
(20)
(11)
A
B
C
I/I0
0
0
0
11 eV shift
7.5 eV shift
50
100
150
Electron Energy (eV)
XBL 727-6583

Fig. 11

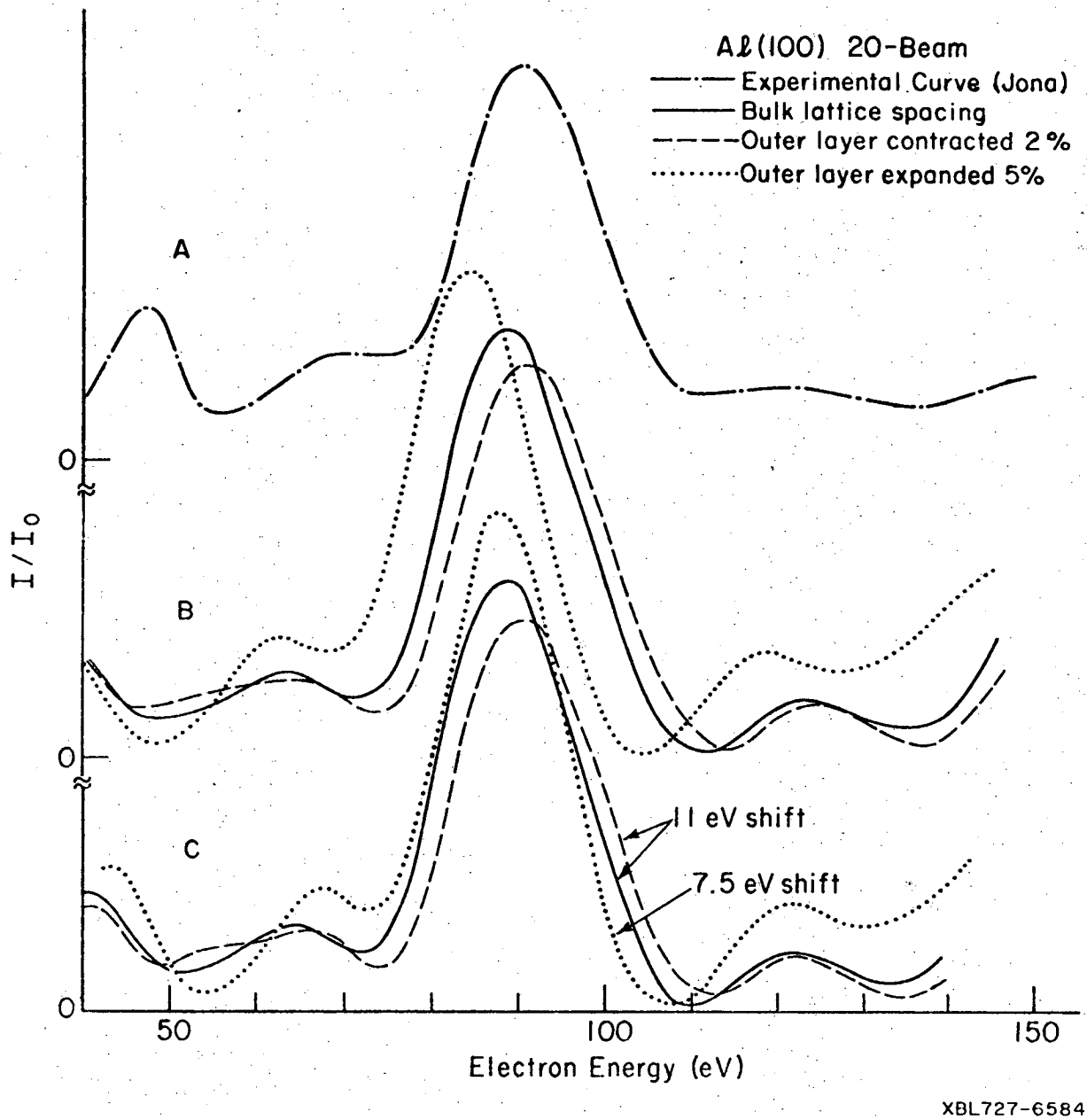
Aℓ(100) 20-Beam
Experimental Curve (Jona)
Bulk lattice spacing
Outer layer contracted 2%
Outer layer expanded 5%
A
B
C
I/I₀
0
0
0
11 eV shift
7.5 eV shift
50
100
150
Electron Energy (eV)
XBL727-6584

Fig. 12

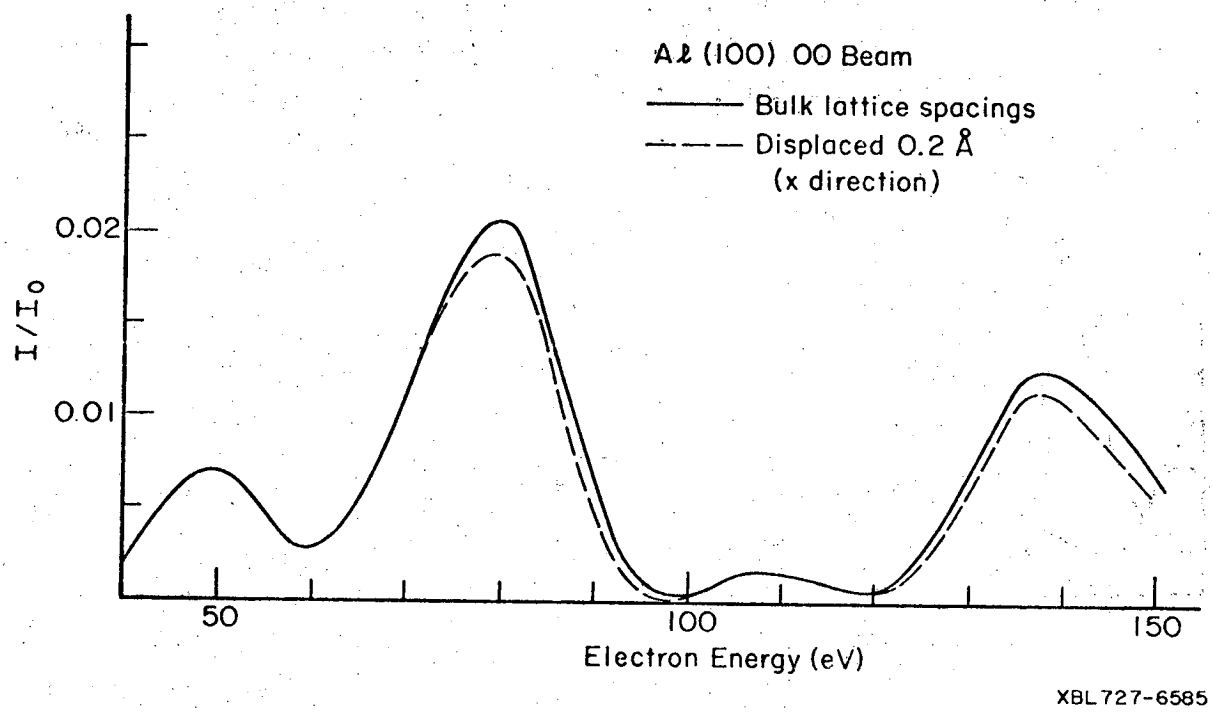
Al (100) 00 Beam
Bulk lattice spacings
Displaced 0.2 Å
(x direction)
0.02
0.01
I/I₀
50
100
150
Electron Energy (eV)
XBL727-6585

Fig. 13

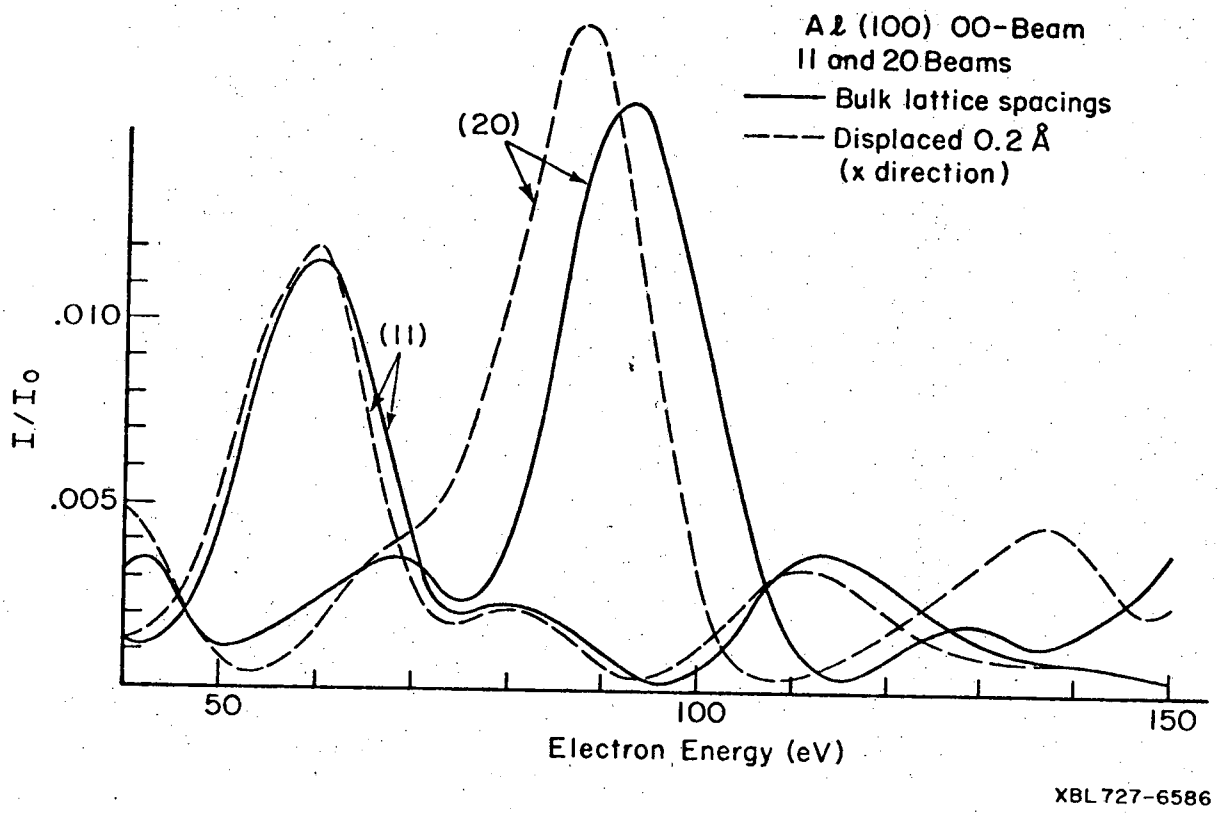
Al (100) 00-Beam
11 and 20 Beams
Bulk lattice spacings
Displaced 0.2 Å
(x direction)
(20)
(11)
.010
.005
I/I₀
50
100
150
Electron Energy (eV)
XBL 727-6586

Fig. 14

TECHNICAL INFORMATION DIVISION
LAWRENCE BERKELEY LABORATORY
UNIVERSITY OF CALIFORNIA
BERKELEY, CALIFORNIA 94720